Hysteresis and change of transition temperature in thin films of $Fe\{[Me_2Pyrz]_3BH\}_2$, a new sublimable spin-crossover molecule

V. Davesne, M. Gruber, M. Studniarek, W. H. Doh, S. Zafeiratos, L. Joly, F. Sirotti, M. G. Silly, A. B. Gaspar, J. A. Real, G. Schmerber, M. Bowen, W. Weber, S. Boukari, V. Da Costa, J. Arabski, W. Wulfhekel, and E. Beaurepaire

Citation: The Journal of Chemical Physics **142**, 194702 (2015); doi: 10.1063/1.4921309
View online: https://doi.org/10.1063/1.4921309
View Table of Contents: http://aip.scitation.org/toc/jcp/142/19
Published by the American Institute of Physics

Articles you may be interested in

Spin crossover in $Fe(phen)_2(NCS)_2$ complexes on metallic surfaces
The Journal of Chemical Physics **146**, 092312 (2017); 10.1063/1.4973511

Study of molecular spin-crossover complex $Fe(phen)_2(NCS)_2$ thin films
Applied Physics Letters **95**, 043303 (2009); 10.1063/1.3192355

Electrical properties and non-volatile memory effect of the $[Fe(HB(pz)_3)_2]$ spin crossover complex integrated in a microelectrode device
Applied Physics Letters **99**, 053307 (2011); 10.1063/1.3616147

First glimpse of the soft x-ray induced excited spin-state trapping effect dynamics on spin cross-over molecules
The Journal of Chemical Physics **139**, 074708 (2013); 10.1063/1.4818603

Microelectromechanical systems integrating molecular spin crossover actuators
Applied Physics Letters **109**, 061903 (2016); 10.1063/1.4960766

Room temperature current modulation in large area electronic junctions of spin crossover thin films
Applied Physics Letters **112**, 013301 (2018); 10.1063/1.5017458

PHYSICS TODAY
WHITEPAPERS
ADVANCED LIGHT CURE ADHESIVES
Take a closer look at what these environmentally friendly adhesive systems can do
READ NOW
PRESENTED BY
MASTERBOND

Hysteresis and change of transition temperature in thin films of $Fe\{[Me_2Pyrz]_3BH\}_2$, a new sublimable spin-crossover molecule

V. Davesne,[1,2] M. Gruber,[1,2] M. Studniarek,[1,3] W. H. Doh,[4] S. Zafeiratos,[4] L. Joly,[1] F. Sirotti,[3] M. G. Silly,[3] A. B. Gaspar,[5] J. A. Real,[5] G. Schmerber,[1] M. Bowen,[1] W. Weber,[1] S. Boukari,[1] V. Da Costa,[1] J. Arabski,[1] W. Wulfhekel,[2] and E. Beaurepaire[1]

[1]*Institut de Physique et de Chimie des Matériaux de Strasbourg, UMR 7504 CNRS, Université de Strasbourg, 23 rue du Loess, 67034 Cedex 2 Strasbourg, France*

[2]*Physikalisches Institut, Karlsruhe Institute of Technology, Wolfgang-Gaede-Str. 1, 76131 Karlsruhe, Germany*

[3]*Synchrotron SOLEIL, L'Orme des Merisiers, Saint-Aubin, BP48, 91192 Gif-sur-Yvette, France*

[4]*Institut de Chimie et Procédés pour l'Energie, l'Environnement et la Santé, UMR 7515 CNRS, Université de Strasbourg, 25 rue Becquerel, 67087 Cedex 2 Strasbourg, France*

[5]*Institut de Ciència Molecular (ICMol), Universitat de València, C/Catedrático José Beltrán Martínez 2, 46980 Paterna (València), Spain*

(Received 31 January 2015; accepted 27 April 2015; published online 18 May 2015)

Thin films of the spin-crossover (SCO) molecule $Fe\{[Me_2Pyrz]_3BH\}_2$ (Fe-pyrz) were sublimed on Si/SiO_2 and quartz substrates, and their properties investigated by X-ray absorption and photoemission spectroscopies, optical absorption, atomic force microscopy, and superconducting quantum interference device. Contrary to the previously studied $Fe(phen)_2(NCS)_2$, the films are not smooth but granular. The thin films qualitatively retain the typical SCO properties of the powder sample (SCO, thermal hysteresis, soft X-ray induced excited spin-state trapping, and light induced excited spin-state trapping) but present intriguing variations even in micrometer-thick films: the transition temperature decreases when the thickness is decreased, and the hysteresis is affected. We explain this behavior in the light of recent studies focusing on the role of surface energy in the thermodynamics of the spin transition in nano-structures. In the high-spin state at room temperature, the films have a large optical gap (~5 eV), decreasing at thickness below 50 nm, possibly due to film morphology. © *2015 AIP Publishing LLC*. [http://dx.doi.org/10.1063/1.4921309]

I. INTRODUCTION

Spin-crossover (SCO) molecules have been the object of many studies[1–4] since their discovery by Cambi and Szegö.[5] This category of metal-organic complexes can undergo a spin transition under the influence of external stimuli (temperature, light,[6–11] ligand-driven,[12] X-rays,[13,14] pressure,[15] magnetic field,[16] and current and electric field[17]). The interest in low-dimensional systems based on spin-crossover molecules has recently seen a significant development,[3,6,18,19] driven by potential technical applications as displays, sensors and memories such as memristors,[17] nano-sized cantilevers, and other emerging applications.[20]

$Fe\{[Me_2Pyrz]_3BH\}_2$ is a compound first reported in 1967[21,22] that exhibits a transition between a S = 0, low-spin (LS) state form and a S = 2, high-spin (HS) state form. Its molecular structure is illustrated in Fig. 1. Light-induced spin state trapping effect (LIESST) has been observed on this molecule[23] in powder, as well as soft X-ray induced spin state trapping effect (SOXIESST) that we have described more in detail in a previous paper.[13] The thermal transition exhibits a hysteresis and a particular asymmetric shape: $T_{HS\rightarrow LS}$ = 174 K and $T_{LS\rightarrow HS}$ = 199 K. The origin of the asymmetric shape is ascribed to a crystal phase transition.[24,25] We attempted temperature dependent X-ray diffraction (XRD) on Fe-pyrz monocrystals but the crystals shattered when the temperature was lowered below the spin transition temperature, which supports a crystal phase transition, as phase changes might exert physical strain on the crystal.

Few known SCO molecules survive a thermal evaporation process in order to prepare high purity nano-objects.[26] This work provides an overview of the characteristics and the intriguing spin transition properties of a new addition to this family, Fe-pyrz, making it an interesting prototype compound for both scientific and industrial applications.

II. METHODS

A. Molecule: Synthesis and deposition

Fe-pyrz was synthesized using a method identical to the one used in our previous study on the powder.[13] The compound was synthesized under Ar atmosphere by adding dropwise 2 mmol of the salt $K[HB(3,5\text{-}(CH_3)_2pz)_3]_2$ dissolved in methanol (15 ml) to a methanolic solution containing 1 mmol of $Fe(BF_4)_2 \cdot 6H_2O$ (5 ml). After complete addition of the $K[HB(3,5\text{-}(CH_3)_2pz)_3]_2$ solution, a white precipitate appears. The precipitate was washed with methanol and dried under vacuum, for a yield of 60%.

We then thermally evaporated Fe-pyrz under high vacuum on clean $Si(100)/SiO_2$ surfaces to see whether the SCO properties are conserved upon sublimation. Additionally, we wanted to check if the thermal hysteresis finds its origin in residual impurities (for example, solvent), or if it

 © 2015 AIP Publishing LLC

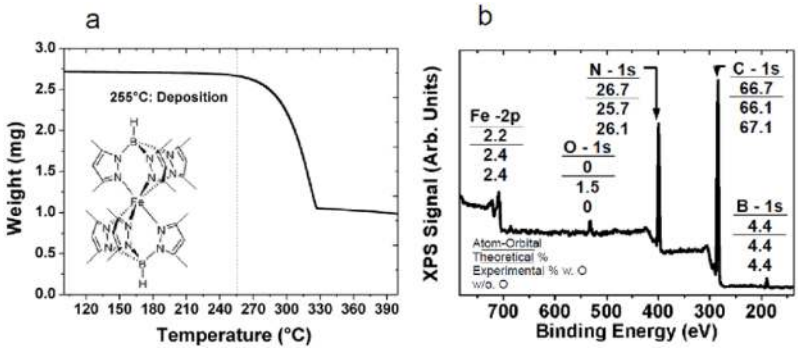

FIG. 1. (a) Thermogravimetric analysis at ambient pressure (air) of the compound noting the deposition temperature used for thermal evaporation experiments, and in the insert, a chemical drawing view of the Fe-pyrz molecule. (b) XPS (Al Kα) elemental analysis of a 620-nm thick Fe-pyrz layer deposited on native SiO_2. The plot corresponds to the XPS spectrum before sputtering, and each peak is identified by its ground state electronic orbital and a quantitative analysis.

is a property inherent to Fe-pyrz. We deposited thick Fe-pyrz films by thermal evaporation (at 255 °C, temperature determined by thermogravimetric analysis presented in Fig. 1) on clean Si(100)/native SiO_2 (named thereafter *native SiO_2*) and Si(100)/thermal 500 nm SiO_2 (named thereafter *thermal SiO_2*) surfaces, and studied them by various analysis techniques. Thicknesses were determined by X-ray reflectometry and profilometry after a first estimation with a quartz microbalance.

B. Characterization methods

Measurements of Fe-pyrz thicknesses were done in a class 100 clean room using a Veeco Dektak 150 surface profiler with a vertical resolution of 5 nm. The atomic force microscopy (AFM) experiments were performed with a Digital Instruments Multimode scanning probe microscope in tapping mode. The experiments were carried out in air and at ambient temperature. The tips were nanosensors non-contact PointProbe Plus - Non-Contact High Frequency silicon tips. The X-ray photoelectron spectroscopy (XPS) measurements were carried out in an ultrahigh vacuum (UHV) setup equipped with a VSW Class WA hemispherical electron analyzer (150 mm radius) with a multi-channeltron detector. A monochromated Al Kα X-ray source (1486.6 eV; anode operating at 240 W) was used as the incident radiation. The surface atomic ratio was calculated by the Fe 2p, O 1s, N 1s, C 1s, and B 1s core level peaks, properly normalized to the photoemission cross section and assuming a homogeneous distribution of these elements on the surface. XRD data for the powder were collected using a Bruker D8 diffractometer equipped with a monochromatic Cu $K\alpha_1$ incident beam (40 kV, 40 mA, $\lambda = 0.154\,056$ nm) and a Sol'X detector. The structural properties of the films were analyzed in the 5°–40° 2θ range by means of a Rigaku Smartlab X-ray diffractometer equipped with a monochromatic source (Ge(220) × 2) delivering a Cu $K\alpha_1$ incident beam (45 kV, 200 mA, $\lambda = 0.154\,056$ nm). A systematic calibration on the Si(400) peak was performed before each measurement. Technical and practical limitations on the nature of the samples made the use of two XRD machines necessary. The X-ray absorption measurements were carried out at the time resolved experiments on materials with photoelectron spectroscopy beamline of synchrotron SOLEIL.[27] X-ray absorption spectroscopy (XAS) spectra were acquired in total electron yield (TEY) mode. The Superconducting QUantum Interference Device (SQUID) results were obtained using a SQUID-VSM (Quantum Design MPMS-XL) magnetometer with magnetic field values up to 7 T. The optical absorption and transmission experiments were performed on a Perkin-Elmer Lambda 950 spectrophotometer. It allows the measurement of the absorption and transmission of UV-visible-near infrared light by thick films or powders with a wavelength resolution of 1 nm. For the thick films of Fe-pyrz deposited on quartz substrates, the absorption and transmission were acquired, and for the powder Fe-pyrz pressed between two quartz plates, the absorption was acquired by measuring the reflectance with an integrating sphere of 150 mm diameter.

III. RESULTS AND DISCUSSION

A. Thermogravimetric and XPS results: Film quality

The thermogravimetric analysis illustrated in Fig. 1(a) exhibits a start of weight loss around 250 °C; therefore, we selected a 255 °C deposition temperature in order to obtain good deposition rates.

As the samples were not characterized *in situ*, it is possible that the surfaces were contaminated by air during transport, despite precautions. This is confirmed by the XPS spectra obtained on samples deposited on native SiO_2 substrates (Fig. 1): they exhibit a peak at O-1s energy, which is a sign of contamination by atmospheric species such as O_2 and H_2O, which might induce oxidation of iron in the film. We rule out O from the SiO_2 substrate since we did not observe a Si-2p peak. We tried to remove the topmost layers with a gentle Ar^+ sputtering, but despite previous successes with $Fe(phen)_2(NCS)_2$ (Fe-phen),[28] this treatment appears destructive to Fe-pyrz layers. The results presented in Fig. 1 were acquired by XPS on a thermal SiO_2//620-nm thick sample. Referring to tabulated atomic cross sections,[29] we could obtain the atomic concentration of the species reported in Fig. 1(b). In the quantitative analysis provided, the first line states the atomic core level, the second line the atomic concentration of the element expected for Fe-pyrz in the layer, the third line the experimental content if we include oxygen, and the fourth line if we do not include it.

If we neglect the oxygen contamination arising from the sample transfer in air, the composition of the layer is the same than that of bulk Fe-pyrz.

B. XRD results: Film structure

Typical XRD data for thin films and the reference powder are presented in Fig. 2. The broad bump for $2\theta \sim 22°$ (respec-

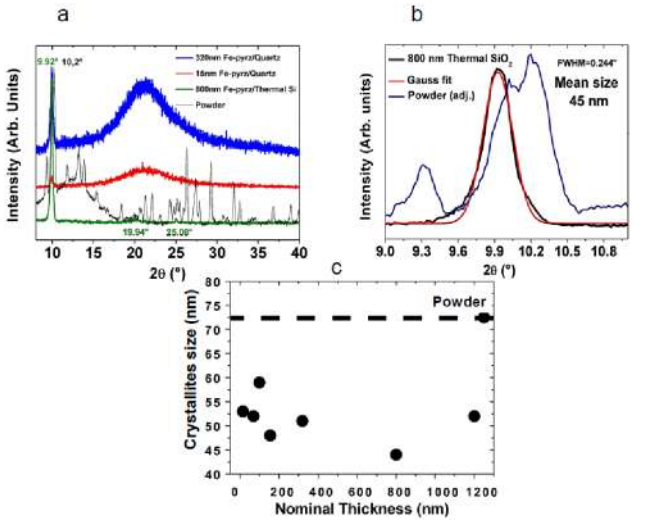

FIG. 2. (a) X-ray diffraction results for various Fe-pyrz thicknesses and substrates, including the powder reference. All spectra were acquired at ambient temperature. (b) is a zoom in plot of the 800 nm-thick sample on the thermal SiO_2, with a gaussian fit of the main peak, used to determine the size of the crystallites using a standard Scherrer equation, and an adjusted spectra of the powder sample to compare the position of the main peaks. (c) This plot is a wider view of the crystallites size as a function of the thickness.

tively, 13°) is characteristic of amorphous quartz substrates (respectively, the sample holder). The powder presents a large number of diffraction peaks in the region of interest that we did not index in detail. The thin films have a leading diffraction peak for $2\theta \sim 9.92°$, slightly shifted from the leading peak of the powder ($2\theta \sim 10.2°$), whose intensity qualitatively scales with the film thicknesses. Moreover, the thickest film presents 2 peaks at $2\theta \sim 19.94°$ and $2\theta \sim 25.08°$ that do not have counterpart in the reference sample. We therefore suggest that the thin films are in a metastable structural organization. More information is gained from the width of the diffraction peaks using the Scherrer equation[30] in order to extract the mean crystallite size τ (Fig. 2). It is found that τ amounts to 50 ± 10 nm for films with thicknesses up to the micrometer range. These values are slightly smaller though comparable to what is found for reference powder ($\tau \sim 70$ nm), suggesting that grain formation of nanometric length scale is a characteristic of Fe-pyrz.

C. AFM results: Film structure and morphology

This crystallite formation is confirmed by AFM topographies of the surface as shown in Fig. 3. Contrary to thermally deposited Fe-phen,[28,31] Fe-pyrz does not exhibit a homogeneous growth on the surface: it forms clusters and crystallites with a typical size 10-200 nm, in agreement with the X-ray data.

At thicknesses below the grain size, the grains are isolated. The formation of grains is a behavior already observed for some other SCO compounds: even if the structure of the molecules is very similar, they may adsorb differently on a surface.[32] Therefore, it is difficult to precisely determine a thickness: the "nominal thicknesses" indicate a quantity of matter deposited on the surface rather than a number of successive layers. We have determined this "nominal thicknesses" of the thicker samples using profilometry and then extrapolated to the thinner

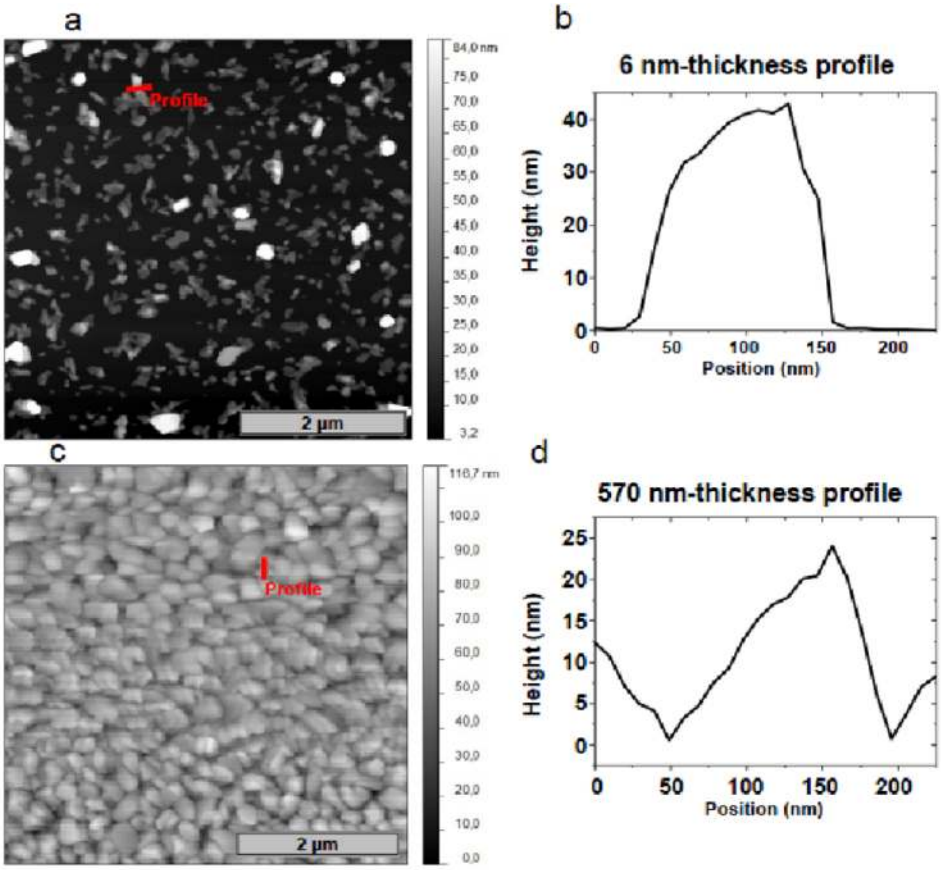

FIG. 3. AFM topographies and height profiles acquired for 6 nm nominal thickness (a) and (b) and 570 nm nominal thickness (c) and (d) on thermal SiO_2.

samples according to the deposition time. Under a nominal thickness of approximately 30 nm, the grains on the surface are then isolated.

For thicker samples, we surmise that there is a formation of successive layers of ~50 nm diameter crystallites, randomly oriented but stacked vertically. Note that the organization of the molecules can be different on metallic crystalline surfaces. We hope that with crystalline surfaces, the layers would be more homogeneous, but results by Mahfoud *et al.*[33] on $Fe(HB(pz)_3)_2$ on Si/SiO_2 that exhibit similar grains prompt us to be cautious. Further studies are expected to clarify this point.

We can obtain more detailed information on the structure of the grains deposited on the surface by image analysis of the 6 nm sample. The distributions represented in Fig. 4 reveal that the crystallites are mostly elongated, and their growth is not isotropic. A log normal fit[34] of the distribution of mean radius of individual gains (the mean distance between the borders of the grain and its barycenter) provides us with a median size of 67 ± 13 nm which is compatible with the X-ray measurements illustrated in Fig. 2. Nonetheless, the dispersion in size and orientation is important.

D. Optical absorption results: Variation of the electronic levels

The layer morphology impacts optical absorption on thick films grown on pure quartz substrates, as illustrated in Fig. 5. The absorption spectra reveal a low absorption in the visible region, consistent with the white-pinkish color of the powder. Absorption of the molecule is much larger in the UV region and the spectra may be viewed as presenting an edge around 250 nm and a tail in the visible part, and thickness fringes for thick samples.

A phenomenological optical band gap can be estimated using Tauc plots: the Tauc formula[35–38] establishes that $(\alpha h\nu)^n = B(h\nu - E_g)$ in the linear part of the Tauc plot, with $\alpha = \ln(1/T)/\text{thickness}$ the absorption coefficient, T the transmission, E_g the optical gap, and B a parameter that gives a measure of the disorder in the crystal.[37] The exponent n can have different values typically in the range of 0.5-3 depending on the nature of the transition. We considered here n as a phenomenological parameter and used a value n = 2 that produces well defined linear sections when plotting $(\alpha h\nu)^2$ as a function of hν (see Fig. 5(b)). We have chosen this method because it is widely used for semi-conductors[36,37] and organic thin films,[39–41] but in our case, we use it in a purely phenomenological purpose, to quantify and highlight the change in energy levels, such as the one that shows up as a "shoulder" in the absorption spectra (inset of Fig. 5(a)).

The use of different n values changes the gap by ~0.3 eV but does not modify the trend observed in Fig. 5.

The effective optical gap is about 4.0 eV for the powder, increases continuously from ~4.7 eV to ~5.0 eV for thick films (from 1200 nm to ~140 nm), and drops to 4.8 eV when we reach discontinouous films below a 60 nm thickness. We believe that the smaller gap of the powder, and for films with thicknesses above 140 nm, might be due to impurities introducing levels in the gap, impurities identified as trace fluor from the reactants.[42] The drop in the optical gap when reaching discontinuous films is a clue of the persistence of interactions between grains in continuous films.

E. SQUID results: Spin transition

The most important question is, however, how does the spin state of thin films switch as compared to bulk samples? This could give insights as the cooperativity mechanisms in such nano-systems. To answer this question, we turn towards SQUID measurements. As evidenced in Fig. 6, the hysteresis and its asymmetry are preserved, and it appears that the spin-transition temperatures shift towards lower temperatures as the film thickness decreases.

This last effect was noted by Palamarciuc *et al.*,[32] observed but not pointed out by Naggert *et al.*[6] in thin films, and interestingly confirmed for nano-crystals by Boldog *et al.*[43] and Martinez *et al.*[44] The results we have obtained are in accordance with theirs, as the nano-crystals also exhibit a decrease in transition temperature. We also observe, like them, a residual HS fraction particularly visible in Fig. 7 and a relative decrease in cooperative behavior and a reduction of the hysteresis, which confirms that the effects we are witnessing find their origin in the grain size and environment

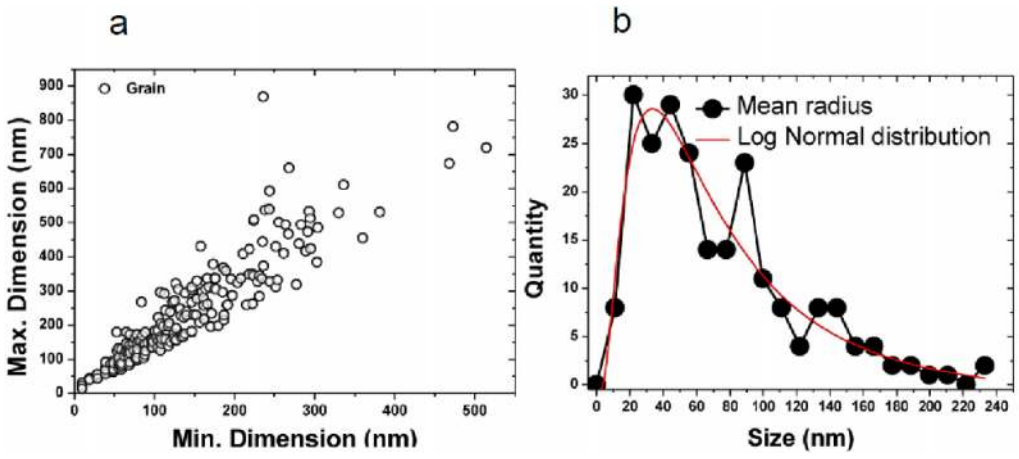

FIG. 4. (a) Graph of the maximum dimension of the grain (or length) as a function of the minimum dimension of the grain (width). (b) Distribution of the mean radius (mean distance between the border of an individual grain and its barycenter) with a log normal distribution (red).

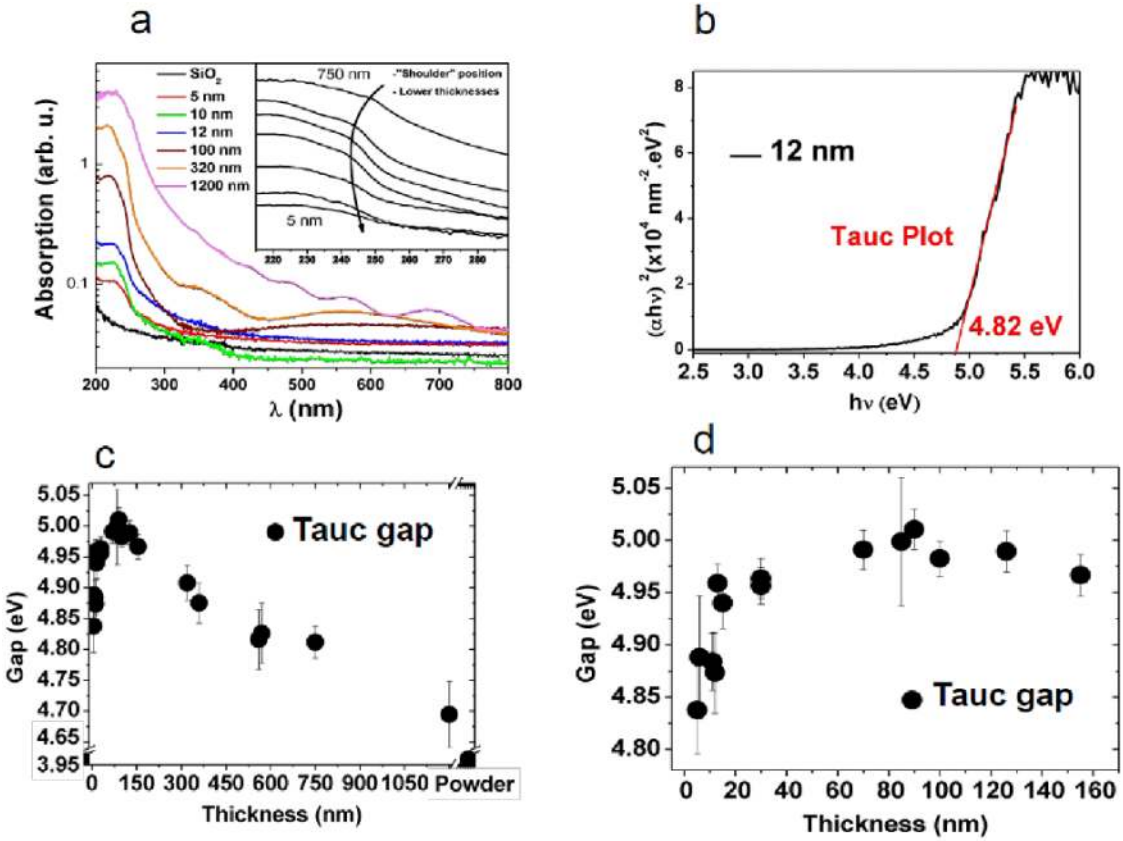

FIG. 5. (a) exhibits the absorption spectra for selected thicknesses of Fe-pyrz deposited on quartz substrate and for the quartz substrate itself, with the absorption on a log scale. The undulation after 300 nm for the thicker films is attributed to interferences. The inset exhibits a zoomed-in portion of the wider plot with selected thicknesses, with an arrow indicating the position of the "shoulder" for decreasing thicknesses. (b) Representation of the effective optical gap (the Tauc plot) for the 12-nm-thick film (black) and the fit of the linear part (red) used to extract the phenomenological optical gap (the Tauc gap). (c) represents the thickness variation of the phenomenological optical gap deduced from the Tauc plots. (d) is a zoom in fraction of the whole bottom plot, focusing on the break at low thicknesses.

of Fe-pyrz nano-crystals. It could be also due to the alteration of the layer by air, as stated previously: more studies will be necessary to understand the full extension of this feature, as we have not yet been able to obtain an acceptable signal/noise ratio for thinner samples. Interestingly, this effect goes in the *opposite* direction for the well-known Fe-phen, which is observable although not mentioned in our previous study.[28]

Also, we have to report two difficulties inherent to such measurements that have a strong impact on our SQUID results of the films: the evaluation of the quantity of molecules in the film and the diamagnetic influence of the substrate. Despite careful measurement of the diamagnetic background of the native SiO_2 substrates after cleaning the substrate with acetone and ethanol from deposited molecules, it is indeed possible that the results are affected by this issue.

In order to provide additional comparison, we have dispersed the powder sample in an alcane glue (eicosane, $C_{20}H_{42}$), and the results exhibit a similar spin-transition temperature shifted towards lower temperatures as in thick films. This suggests a significant influence of the environment of Fe-pyrz on the spin transition, as eicosane glue adds another interaction between the particles and the matrix.[45]

Regarding nano-sized monocrystals, recent studies have suggested that the change in transition temperature is in fact due to differing surface tensions for both spin states of the molecule, reducing the transition temperature and the hysteresis.[46,47] This can also explain the different behaviors of

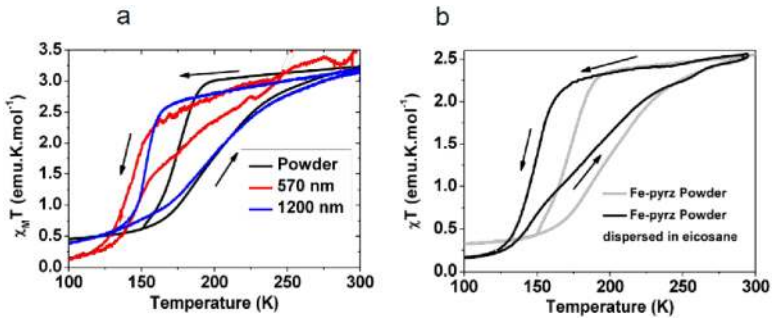

FIG. 6. The (a) plot presents SQUID magnetic susceptibility results for two thick films thicknesses (570 nm and 1200 nm on native SiO_2) compared to the powder reference, with the arrows identifying the direction of the temperature sweep. The molecules exhibit a shift in spin transition temperature towards lower temperatures with decreasing thicknesses. The (b) plot presents the results for the powder, in this specific example dispersed in eicosane (purely alcane) glue.

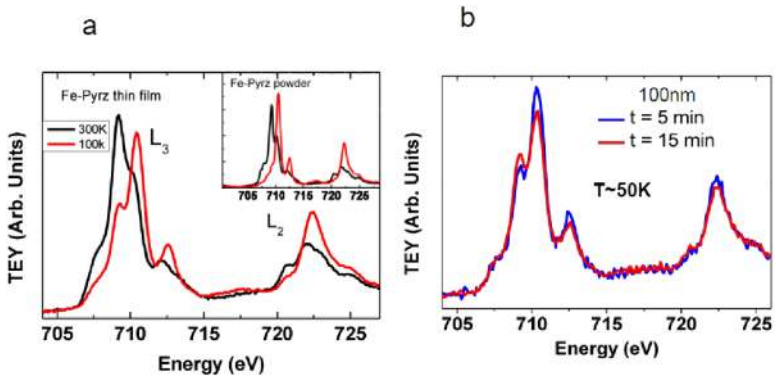

FIG. 7. (a) XAS spectra of the Fe-pyrz Fe L-edges for the powder reference (HS acquired at 245 K and LS at 80 K) and the 100 nm thin film, normalized to the same integral, for temperatures above and below the spin-transition temperature. The ambient temperature spectra are clearly similar, while the low temperature thin film spectra visibly retain an estimated 24% HS-state. (b) XAS Fe L-edge spectra acquired on Fe-pyrz thin-film for different X-ray illumination times of the sample at ~50 K. Due to the SOXIESST effect, the HS-state proportion increases.

Fe-phen and Fe-pyrz: the surface tensions of the LS molecule are higher than that of the HS molecule for Fe-pyrz, and the contrary for Fe-phen, which favor the HS state at the interface for Fe-pyrz, and the LS state for Fe-phen. The results exhibited in Fig. 6 offer an experimental confirmation to these theoretical insights.

We suggest that the relative high thickness at which we observe this shift might be due to a two-level cooperative behavior: between the molecules inside a grain and between the grains inside a layer. Indeed, as the spin transition in Fe-pyrz has been suggested to trigger a phase transition that can shatter a monocrystal, we believe that it is possible that the pressure exerted by grains on each other might alter the spin-transition temperature. With this in mind, we should consider the contribution of interface particles compared to the bulk: at a conservative estimate of 50 nm-particle size, the contribution of interface (with the surface and with the substrate) particles is ~8% for the 1200 nm sample and 18% for the 570 nm sample, which could explain the difference between the HS → LS transition temperatures of 153 K and 144 K, respectively.

F. XAS results: Spin-transition completeness

Further information on the layers can be obtained by XAS, with the TEY acquisition mode, a technique that is particularly adapted to the study of SCO thin films.[13,48] By comparing in Fig. 7(a) the reference spectra acquired with the powder sample and the thick-film sample spectra at 100 K and 300 K, we can observe two points: (a) the spectra change from LS-type to HS-type,[13,49,50] indicating a spin transition; (b) the spin transition is not complete at low temperature, as part of the thick-film sample (~20%) seems "HS-pinned" and do not switch. This behavior is known among spin-transition compounds and is believed to arise from the interaction with the surface.[31,51] The spin transition seems preserved. Moreover, the HS-state proportion might increase compared to the LS-state proportion when applying X-rays at low temperature due to the SOXIESST as described recently for such systems.[13] This is illustrated in Fig. 7(b) that shows a slight increase of the HS contribution at 50 K when the exposure time of the film to X-rays increases from 5 to 15 min.

G. XAS results: Light and soft X-ray induced spin transition

Another route to trigger the spin transition is the optical excitation at low temperature of LS state Fe-pyrz to a metastable HS state via the LIESST effect.[6,10,52] Typically for most Fe^{2+} systems, the LS → HS transition is obtained for light excitation in the UV-blue wavelength, whereas the reverse transition HS → LS takes place for longer wavelength (~600 nm). In order to study this effect, we measured the time dependence of Fe L_3 XAS spectra using the procedure described in Ref. 13.

Fig. 8 shows that optical excitation leads to slow dynamics (i.e., on minute time scales) toward the HS state, though the transition remains incomplete even at high light intensity. In addition, the laser illumination seems much more efficient than the diode. This might be due to (i) the opposing processes of relaxation and excitation in a low-cooperative environment, a phenomenon that was already noted in the bulk form when comparing to Fe-phen,[13] and/or to (ii) the presence of reverse-LIESST due to the wide excitation spectra delivered by the light emitting diode (LED) compared to the laser, and/or to (iii) local heating by the laser, and/or (iv) the presence of "LS-pinned" molecules in the thin film.

For qualitative purposes, we provide the parameters of a fit of the two LIESST time dependencies based on the procedure

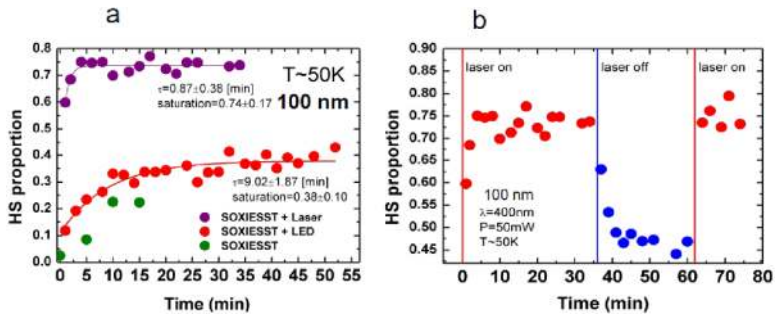

FIG. 8. (a) LIESST effect within a probed region of Fe-Pyrz 100 nm thin film, acquired while irradiating the sample with white LED or Ti:sapphs pulse laser (50 mW, estimated 100 fs pulse). Irradiating with the laser results in a more abrupt phenomenon with higher level of saturation than with the LED. (b) Reversible HS proportion switching of Fe-Pyrz thin film by successively turning the laser on and off.

described in Ref. 13. The dynamics of the system regarding LIESST and SOXIESST seems slow enough to be investigated conjointly, which open perspectives, for example, Fig. 8(b), present the results of LIESST by the laser on a thin film already partially excited (45%) by SOXIESST.

However, as we have already discussed in our previous study,[13] quantitative dynamics results and especially meaningful comparison between studies require careful assessment of light and X-ray illumination parameters (wavelength, intensity, and beam structure), and since our previous study was held with different parameters, we cannot quantitatively compare thin film and powder dynamics. Combined with the particular transition properties of Fe-pyrz thin films, the LIESST effect on Fe-pyrz thin films opens perspectives for the use of the system as switches or sensors.

IV. CONCLUSION AND PERSPECTIVE

We have deposited Fe-pyrz onto Si/SiO_2 substrates for the first time. Contrary to the previously studied $Fe(phen)_2(NCS)_2$, the films tend to form crystallites rather than continuous films. A possible consequence of this behavior is the decrease of the optical gap below 50 nm. The thin films qualitatively retain the typical characteristics encountered in powder samples (spin-crossover, hysteresis, SOXIESST, and LIESST) but present intriguing variations: the transition temperature decreases when the thickness is decreased, and the hysteresis is affected. The molecules (respectively, nanocrystals) at the surface of low-dimensional spin transition systems behave differently as the molecules (respectively, nanocrystals) in the bulk of the grain (respectively, layer), giving rise to a different macroscopic spin transition behavior. It is difficult to exactly model the change applicable to our system based on the simple equations used in these works, since the spin transition of Fe-pyrz is asymmetric and still not fully understood, but what is particularly unexpected is the high nominal thickness at which it is still possible to observe the effect, compared to theoretical work on surface tension effects in SCO molecules. We surmise that this is due to the nanocrystalline growth of the molecule on our substrate: the dimensions of individual crystals seem to be small enough to maintain a high surface area, and therefore a significant decrease in the spin-transition temperature. We suggest that the cooperative behavior happens not only between the molecules in a grain but also between grains in a film. This dependence of the transition temperature on the thickness of the layer that still presents a significant effect at high thicknesses can easily be harnessed to use in organic spintronic devices, such as heat sensors.[42]

ACKNOWLEDGMENTS

We would like to thank R. Bernard for his help in the clean room. We thank B. Muller, A. Boulard, B. Leconte, Y. T. Law, and C. Kieber for technical assistance, and A. Derory for SQUID measurements. We thank F. Scheurer for useful discussions and advices. We acknowledge funding from the Franco-German university, from the Baden-Württemberg Stiftung in the framework of the Kompetenznetz für Funktionale Nanostrukturen (KFN) and from the Agence Nationale de la Recherche No. ANR-11-LABX-0058 NIE and from the International Center for Frontier Research in Chemistry. The Spanish Ministerio de Ciencia e Innovaciónn (MICINN) and the Generalitat Valenciana through Project Nos. CTQ2013-46275-P and PROMETEO/2012/049 are acknowledged.

[1]P. Gütlich and H. A. Goodwin, in *Spin Crossover in Transition Metal Compounds I*, edited by P. Gütlich and H. A. Goodwin (Springer Berlin Heidelberg, Berlin, Heidelberg, 2004), pp. 1–47.
[2]P. Gütlich, Y. Garcia, and H. A. Goodwin, Chem. Soc. Rev. **29**, 419 (2000).
[3]J. A. Real, A. B. Gaspar, and M. C. Muñoz, Dalton Trans. **12**, 2062 (2005).
[4]K. S. Murray, in *Spin-Crossover Materials*, edited by M. A. Halcrow (John Wiley & Sons, Ltd, 2013), pp. 1–54.
[5]L. Cambi and L. Szegö, Ber. Dtsch. Chem. Ges. B Ser. **64**, 2591 (1931).
[6]H. Naggert, A. Bannwarth, S. Chemnitz, T. von Hofe, E. Quandt, and F. Tuczek, Dalton Trans. **40**, 6364 (2011).
[7]A. Cannizzo, C. J. Milne, C. Consani, W. Gawelda, C. Bressler, F. van Mourik, and M. Chergui, Coord. Chem. Rev. **254**, 2677 (2010).
[8]R. Herber and L. M. Casson, Inorg. Chem. **25**, 847 (1986).
[9]A. Hauser, in *Spin Crossover in Transition Metal Compounds II*, edited by P. Gütlich and H. A. Goodwin (Springer Berlin Heidelberg, Berlin, Heidelberg, 2004), pp. 155–198.
[10]S. Decurtins, P. Gutlich, K. M. Hasselbach, A. Hauser, and H. Spiering, Inorg. Chem. **24**, 2174 (1985).
[11]A. Hauser, Chem. Phys. Lett. **6**, 543 (1986).
[12]M.-L. Boillot, J. Zarembowitch, and A. Sour, in *Spin Crossover in Transition Metal Compounds II*, edited by P. Gütlich and H. A. Goodwin (Springer Berlin Heidelberg, Berlin, Heidelberg, 2004), pp. 261–276.
[13]V. Davesne, M. Gruber, T. Miyamachi, V. D. Costa, S. Boukari, F. Scheurer, L. Joly, P. Ohresser, E. Otero, F. Choueikani, A. B. Gaspar, J. A. Real, W. Wulfhekel, M. Bowen, and E. Beaurepaire, J. Chem. Phys. **139**, 074708 (2013).
[14]D. Collison, C. D. Garner, C. M. McGrath, J. F. W. Mosselmans, M. D. Roper, J. M. W. Seddon, E. Sinn, and N. A. Young, J. Chem. Soc., Dalton Trans. **22**, 4371 (1997).
[15]V. Ksenofontov, A. B. Gaspar, and P. Gütlich, in *Spin Crossover in Transition Metal Compounds III*, edited by P. Gütlich and H. A. Goodwin (Springer Berlin Heidelberg, Berlin, Heidelberg, 2004), pp. 23–64.
[16]A. Bousseksou, F. Varret, M. Goiran, K. Boukheddaden, and J. P. Tuchagues, in *Spin Crossover in Transition Metal Compounds III*, edited by P. Gütlich and H. A. Goodwin (Springer Berlin Heidelberg, Berlin, Heidelberg, 2004), pp. 65–84.
[17]T. Miyamachi, M. Gruber, V. Davesne, M. Bowen, S. Boukari, L. Joly, F. Scheurer, G. Rogez, T. K. Yamada, P. Ohresser, E. Beaurepaire, and W. Wulfhekel, Nat. Commun. **3**, 938 (2012).
[18]P. N. Martinho, C. Rajnak, and M. Ruben, in *Spin-Crossover Materials*, edited by M. A. Halcrow (John Wiley & Sons, Ltd, 2013), pp. 375–404.
[19]A. Pronschinske, Y. Chen, G. F. Lewis, D. A. Shultz, A. Calzolari, M. Buongiorno Nardelli, and D. B. Dougherty, Nano Lett. **13**, 1429 (2013).
[20]G. Molnár, L. Salmon, W. Nicolazzi, F. Terki, and A. Bousseksou, J. Mater. Chem. C **2**, 1360 (2014).
[21]J. P. Jesson, S. Trofimenko, and D. R. Eaton, J. Am. Chem. Soc. **89**, 3148 (1967).
[22]J. P. Jesson, S. Trofimenko, and D. R. Eaton, J. Am. Chem. Soc. **89**, 3158 (1967).
[23]L. Capes, J.-F. Létard, and O. Kahn, Chem. - Eur. J. **6**, 2246 (2000).
[24]N. Bréfuel, H. Watanabe, L. Toupet, J. Come, N. Matsumoto, E. Collet, K. Tanaka, and J.-P. Tuchagues, Angew. Chem., Int. Ed. **48**, 9304 (2009).
[25]M. Seredyuk, M. C. Muñoz, M. Castro, T. Romero-Morcillo, A. B. Gaspar, and J. A. Real, Chem. - Eur. J. **19**, 6591 (2013).
[26]A. Bousseksou, G. Molnár, L. Salmon, and W. Nicolazzi, Chem. Soc. Rev. **40**, 3313 (2011).
[27]F. Polack, M. Silly, C. Chauvet, B. Lagarde, N. Bergeard, M. Izquierdo, O. Chubar, D. Krizmancic, M. Ribbens, J.-P. Duval, C. Basset, S. Kubsky, F. Sirotti, R. Garrett, I. Gentle, K. Nugent, and S. Wilkins, AIP Conf. Proc. **1234**, 185–188 (2010).
[28]S. Shi, G. Schmerber, J. Arabski, J.-B. Beaufrand, D. J. Kim, S. Boukari, M. Bowen, N. T. Kemp, N. Viart, G. Rogez, E. Beaurepaire, H. Aubriet, J. Petersen, C. Becker, and D. Ruch, Appl. Phys. Lett. **95**, 043303 (2009).
[29]D. Briggs and M. P. Seah, in *Practical Surface Analysis, Auger and X-Ray Photoelectron Spectroscopy* (Wiley, Chichester, New York, 1996), Vol. 1.
[30]J. I. Langford and A. J. C. Wilson, J. Appl. Crystallogr. **11**, 102 (1978).

[31]M. Gruber, V. Davesne, M. Bowen, S. Boukari, E. Beaurepaire, W. Wulfhekel, and T. Miyamachi, Phys. Rev. B **89**, 195415 (2014).
[32]T. Palamarciuc, J. C. Oberg, F. E. Hallak, C. F. Hirjibehedin, M. Serri, S. Heutz, J.-F. Létard, and P. Rosa, J. Mater. Chem. **22**, 9690 (2012).
[33]T. Mahfoud, G. Molnár, S. Cobo, L. Salmon, C. Thibault, C. Vieu, P. Demont, and A. Bousseksou, Appl. Phys. Lett. **99**, 053307 (2011).
[34]O. G. Raabe, J. Aerosol Sci. **2**, 289 (1971).
[35]J. Tauc, R. Grigorovici, and A. Vancu, Phys. Status Solidi B **15**, 627 (1966).
[36]J. Tauc, *Amorphous and Liquid Semiconductors* (Plenum, 1974).
[37]R. Moubah, S. Colis, M. Gallart, G. Schmerber, P. Gilliot, and A. Dinia, J. Lumin. **132**, 457 (2012).
[38]R. Moubah, *Structure et Magnétisme Des Couches Minces de Cobaltite de Types $Ca_3Co_2O_6$ et $Ca_3Co_4O_9$ Déposées Par Ablation Laser Pulsée* (Université de Strasbourg, Strasbourg, 2010).
[39]F. Yakuphanoglu and M. Sekerci, Opt. Appl. **35**, 209 (2005).
[40]F. Yakuphanoglu, M. Sekerci, and A. Balaban, Opt. Mater **27**, 1369 (2005).
[41]M. E. Sánchez-Vergara, J. C. Alonso-Huitron, A. Rodriguez-Gómez, and J. N. Reider-Burstin, Molecules **17**, 10000 (2012).
[42]V. Davesne, *Organic Spintronics: An Investigation on Spin-Crossover Complexes from Isolated Molecules to the Device* (Universität Karlsruhe/Université de Strasbourg, 2013).
[43]I. Boldog, A. B. Gaspar, V. Martínez, P. Pardo-Ibañez, V. Ksenofontov, A. Bhattacharjee, P. Gütlich, and J. A. Real, Angew. Chem., Int. Ed. **47**, 6433 (2008).
[44]V. Martínez, I. Boldog, A. B. Gaspar, V. Ksenofontov, A. Bhattacharjee, P. Gütlich, and J. A. Real, Chem. Mater. **22**, 4271 (2010).
[45]R. Tanasa, J. Laisney, A. Stancu, M.-L. Boillot, and C. Enachescu, Appl. Phys. Lett. **104**, 031909 (2014).
[46]G. Félix, W. Nicolazzi, L. Salmon, G. Molnár, M. Perrier, G. Maurin, J. Larionova, J. Long, Y. Guari, and A. Bousseksou, Phys. Rev. Lett. **110**, 235701 (2013).
[47]M. Mikolasek, G. Félix, W. Nicolazzi, G. Molnár, L. Salmon, and A. Bousseksou, New J. Chem. **38**, 1834 (2014).
[48]M. Bernien, "X-Ray absorption spectroscopy of Fe complexes on surfaces: Electronic interactions and tailoring of the magnetic coupling," Ph.D. thesis (Freie Universität Berlin, Germany, 2009).
[49]C. Cartier dit Moulin, P. Rudolf, A. M. Flank, and C. T. Chen, J. Phys. Chem. **96**, 6196 (1992).
[50]V. Briois, C. C. dit Moulin, P. Sainctavit, C. Brouder, and A.-M. Flank, J. Am. Chem. Soc. **117**, 1019 (1995).
[51]S. Gueddida and M. Alouani, Phys. Rev. B **87**, 144413 (2013).
[52]J.-F. Létard, L. Capes, G. Chastanet, N. Moliner, S. Létard, J.-A. Real, and O. Kahn, Chem. Phys. Lett. **313**, 115 (1999).